Molecular and Cellular Endocrinology 307 (2009) 185–195

Contents lists available at ScienceDirect

Molecular and Cellular Endocrinology

journal homepage: www.elsevier.com/locate/mce

Digital fluorescence analysis of trafficking of single endosomes containing low-density lipoprotein in adrenocortical cells: Facilitation of centripetal motion by adrenocorticotropic hormone

Tetsuya Kimoto[a,b,1], Makoto Yamada[a,b,c,1], Tomomitsu Ichikawa[a], Daisaku Honma[a], Richard J. Cherry[d], Ian E.G. Morrison[d], Suguru Kawato[a,b,*]

[a] Department of Biophysics and Life Sciences, Graduate School of Arts and Sciences, The University of Tokyo, 3-8-1 Komaba, Meguro, Tokyo 153-8902, Japan
[b] Core Research for Evolutional Science and Technology Project of Japan Science and Technology Agency, The University of Tokyo, Japan
[c] Department of Physics, School of Medicine, Kyorin University, Mitaka, Tokyo 181-8611, Japan
[d] Department of Biological Sciences, University of Essex, Central Campus, Colchester CO4 3SQ, UK

ARTICLE INFO

Article history:
Received 11 January 2009
Received in revised form 22 April 2009
Accepted 24 April 2009

Keywords:
Fluorescence imaging
LDL
Adrenocortical cells
Endosome
Single particle tracking
ACTH

ABSTRACT

Imaging of trafficking of endosomes containing low-density lipoprotein (LDL) is useful to analyze cholesterol transport in adrenocortical cells. At 60 min after the application of fluorescently labeled LDL to adrenocortical cells, individual endosomes containing LDL were demonstrated to undergo frequent switching between forward and reverse movement and immobility. The population of moving endosomes ($\geq$0.065 μm/s) was approximately 75% in control cells. The remaining endosomes were either slowly moving or temporarily immobile. At 3 h after the LDL addition, endosomes were concentrated around the circumference of the cell nuclei. The endosome movement was inhibited by nocodazole, implying that endosomes undergo movement along microtubule networks. Anti-dynein antibodies inhibited the motion of endosomes towards the nucleus, and anti-kinesin antibodies inhibited peripherally directed motion. These results imply that both dynein-like and kinesin-like motor proteins bind to the same endosome, resulting in saltatory movements with centripetal or peripherally directed direction, depending on which motor binds to microtubules. Though the dynein and kinesin motors drive the endosomes very rapidly (μm/s), frequent saltatory motions of single endosomes may induce the very slow net centripetal motion (μm/h).The application of adrenocorticotropic hormone (ACTH) resulted in a facilitation of the centripetal motion of endosomes, resulting in the establishment of the concentration of endosomes around cell nuclei within 1 h.

1. Introduction

Steroid hormones produced in adrenocortical cells play a key role in gluconeogenesis, homeostasis of Na^+/K^+ concentration, and the suppression of inflammation. In the inner mitochondrial membrane, free cholesterol is converted to pregnenolone (PREG) by cytochrome P450 side-chain cleavage enzyme (P450scc; CYP11A1). PREG is metabolized further in endoplasmic reticulum and mitochondria, by 3β-hydroxysteroid dehydrogenase, P45017α(CYP17), P450c21 (CYP21) and P45011β (CYP11B1), resulting in glucocorticoid production in fasciculata cells. The increase in the rate of glucocorticoid synthesis is provoked by adrenocorticotropic hormone (ACTH) secreted from anterior pituitary in response to stress (Kimura, 1981; Jacobson, 2005). Upon the rapid activation of steroidogenesis, the accompanying signal transduction pathway may occur sequentially through: (1) hormone receptors in the plasma membrane; (2) Ca^{2+} signaling in the cytoplasm (Kimoto et al., 1996) and/or cAMP signaling (Grahame-Smith et al., 1967) (3) transport of free cholesterol via steroidogenic acute regulatory (StAR) protein and/or peripheral-type benzodiazepine receptors from the outer to the inner mitochondrial membranes (Massotti et al., 1991; Cavallaro et al., 1993; King et al., 1995; Stocco and Clark, 1996) and (4) conversion of cholesterol to PREG by P450scc. ACTH also induces the up-regulation of P450scc and other steroidogenic enzymes, which supports the prolonged steroidogenesis lasting for several hours to days (Simpson and Waterman, 1983).

For the sustained steroidogenesis, a constant supply of cholesterol to mitochondria is required. The potential sources of cholesterol in adrenocortical cells are (1) cholesteryl esters pooled

* Corresponding author at: Department of Biophysics and Life Sciences, Graduate School of Arts and Sciences, The University of Tokyo, 3-8-1 Komaba, Meguro, Tokyo 153-8902, Japan. Tel.: +81 3 5454 6517; fax: +81 3 5454 6517.
E-mail address: kawato@phys.c.u-tokyo.ac.jp (S. Kawato).
[1] These two authors contributed equally to this work.

0303-7207/$ – see front matter © 2009 Elsevier Ireland Ltd. All rights reserved.
doi:10.1016/j.mce.2009.04.016

in lipid droplets, (2) cholesteryl esters derived from low-density lipoprotein (LDL) (Kovanen et al., 1979), (3) cholesteryl esters taken up from high-density lipoprotein via scavenger receptor class B type I (Glass et al., 1983; Connelly and Williams, 2003) and/or (4) cholesterol synthesized *de novo* by enzymes such as 3-hydroxy-3-methylglutaryl coenzyme A (HMG-CoA) reductase. The supply of cholesteryl esters via LDL may contribute to slow phase but not to acute phase of steroidogenesis, because LDL enhances steroidogenesis only after 4 h of the addition, but not within 2 h in ACTH-stimulated adrenocortical cells (Yaguchi et al., 1998). It has also been shown in LDL receptor-knock out mice that the supply of cholesteryl esters via LDL receptors is not necessary to the ACTH-induced acute steroidogenesis (Kraemer et al., 2007). Because the application of LDL restores the volume of lipid droplets pre-depleted with ACTH (Heikkila et al., 1989), cholesteryl esters conveyed by LDL may be used for restoration of intracellular cholesterol pools. In response to the stimulation of ACTH, cholesteryl esters are hydrolyzed by hormone-sensitive lipase in lipid droplets (Li et al., 2002), and the generated free cholesterol is provided to mitochondria. However, mitochondrial cholesterol and cholesteryl esters in lipid droplets are quickly depleted in response to ACTH (Glick and Ochs, 1955; Dietschy et al., 1983). Moreover, *de novo* synthesis of cholesterol is not sufficient for optimal steroidogenesis induced by ACTH (Iwaki et al., 1985). The activity of HMG-CoA reductase can be up-regulated by ACTH as a compensation of lipoprotein deficiency, however, the effect is inhibited by LDL which is provided from circulation (Rainey et al., 1992). Taken together, exogenous supply of cholesteryl esters via LDL seems to be necessary for sustained slow steroidogenesis in ACTH-stimulated adrenocortical cells.

LDL is incorporated into early endosomes via LDL receptor-mediated endocytosis (Kovanen et al., 1979). LDL–receptor complex is transported further from the early to the late endosomes (which might be associated with lysosomes) by endosomal carrier vesicles (ECVs) (Griffiths, 1996). LDL is digested in late endosomes/lysosomes locating in the perinuclear region (Simpson and Waterman, 1983; Paavola et al., 1985). As stated above, the regulation of intramitochondrial cholesterol transport by ACTH and of the supply of cholesterol from lipid droplets to mitochondria has been extensively investigated. However, the regulation in the early stage of the intracellular cholesterol transport carried by LDL remains largely unknown. Though ACTH induces the increase of LDL receptors and LDL uptake (Kovanen et al., 1979; Kroon et al., 1984), it is not known whether the transport of LDL is under the regulation by ACTH. Therefore, we here investigate the intracellular LDL transport process by ECVs. In the current study, video-enhanced digital fluorescence microscopy is employed, in order to trace the change in distribution of endosomes. This methodology is used for the analysis of endosome movement in rat ovarian granulosa cells (Herman and Albertini, 1984) and HEp2 cells (Ghosh and Maxfield, 1995). Furthermore, we analyze images with a single endosome tracking method, in order to trace the rapid multidirectional motions of individual endosomes, because these motions are the elemental steps of the resulting slow perinuclear concentration of endosomes, as shown in rat hippocampal glial cells (Ichikawa et al., 2000).

2. Materials and methods

2.1. Materials

Dioctadecyl tetramethylindocarbocyanine perchlorate (DiI) was purchased from Molecular Probes (Eugene, OR), ACTH 1-24 peptide (Cortrosyn) from Dai-ichi Seiyaku (Tokyo, Japan), and gentamicin sulfate from Schering-Plough (Tokyo, Japan). Powdered F-10 (Ham) medium, fetal calf serum, and horse serum was obtained from GIBCO (Rockville, MD). Newborn calf serum was from BioProducts (West Sacramento, CA). L-Glutamine was from BioWittaker (Walkersville, MD). Acridine orange, sodium orthovanadate, forskolin, BAPTA/AM, and saponin were from Wako (Osaka, Japan). 5′-adenylyl imidodiphosphate (AMP-PNP), cytochalasin D and nocodazole were purchased from Sigma–Aldrich (St Louis, MO). Cy2-conjugated goat anti-mouse IgG antibodies and monoclonal anti-alpha tubulin antibodies were purchased from Amersham (Buckinghamshire, UK). Monoclonal anti-dynein antibodies (clone No. 70.1) were from Sigma. Monoclonal antibodies against kinesin heavy chain (clone SUK-4) were from BabCO (Richmond, CA). Glass-bottom dishes were obtained from MatTek (Ashland, MA). Trilostane and SU-10603 were provided from Mochida Pharmaceutical (Tokyo, Japan) and Novartis (Basel, Switzerland), respectively. Antibody against PREG was gifted by Dr. T. Yamazaki at Hiroshima University. [7-^{3}H]PREG (23.5 Ci/mmol) was obtained from NEN Life Science Products (Boston, MA). All other chemicals were of the highest purity commercially available.

2.2. LDL isolation

LDL was isolated from fresh bovine blood via a modified version of the method of Havel et al. (Havel et al., 1955; Ichikawa et al., 2000), using sequential differential floatation in sodium chloride (density, $d = 1.006$) and sodium bromide solutions ($d = 1.063$), with ultra-centrifugation at 200,000 × g and 16 °C. The resultant LDL-containing supernatant was dialyzed against 150 mM NaCl, 20 mM HEPES and 0.01% EDTA (pH 7.4) at 4 °C, overnight. The sample was stored at 4 °C under nitrogen until used. All LDL samples were used within 7 days of isolation to avoid denaturation. LDL fraction purity was confirmed using sodium dodecylsulfate (SDS)-polyacrylamide gel electrophoresis, which yielded a clear, single band. Protein concentration was determined by BCA Protein Assay kit (Pierce, Rockford, IL) using bovine serum albumin (BSA) as a standard.

2.3. Labeling of LDL with DiI

DiI was dissolved in DMSO, and 400 μL of the solution (2 mM) was incubated for 2 h with 1.6–1.9 mg/mL of LDL, in a total volume of 3 mL at room temperature (Ichikawa et al., 2000). Free DiI was removed from labeled LDL by centrifuge gel filtration with a Sephadex G-25 column (Pharmacia, Sweden). For each column, 250 μL of the suspension was applied and centrifuged at 900 × g for 3 min. The applied elution buffer was 20 mM HEPES (pH 7.4), containing 150 mM NaCl. Approximately 16 DiI molecules were bound to each LDL molecule.

2.4. Preparation of adrenocortical cell cultures

Bovine adrenal glands were obtained from a local slaughterhouse. Adrenocortical zona fasciculata-reticularis cells were aseptically isolated by collagenase-DNase digestion as described elsewhere (Kimoto et al., 1996, 1997). Briefly, the cortical tissue was minced and digested with collagenase (0.1%) and DNase I (0.005%) in a Krebs-Ringer bicarbonate glucose buffer containing 125 mM NaCl, 6 mM KCl, 1.2 mM KH_2PO_4, 1.2 mM $MgSO_4$, 1.2 mM $CaCl_2$, 0.01 mM EGTA, 25.3 mM $NaHCO_3$, 0.2% glucose, 0.3% BSA, and 0.005% gentamicin (pH 7.4). The digestion was performed for 1 h at 37 °C under an O_2/CO_2 gas (95%/5%). Isolated cells were cultured in Ham's F-10 medium supplemented with 5% fetal calf serum, 10% newborn calf serum, 2.5% horse serum, 100 U/mL penicillin G, 100 μg/mL streptomycin, and 50 μg/mL gentamicin. The culture medium was renewed on the second day of the culture. Cells were placed onto 35 mm ϕ glass-bottom dishes coated with collagen. For microscopic studies, cells were cultured for 4–5 days at a cell density of 0.8×10^4 cells/cm^2. Cell viability was better than 95%, as determined by the trypan blue exclusion test.

2.5. Incorporation of labeled LDL in adrenocortical cells

The observation medium (PS medium) contained 10 mM Na-HEPES (pH 7.4), 120 mM NaCl, 4 mM KCl, 1 mM NaH_2PO_4, 1.25 mM $CaCl_2$, 0.5 mM $MgSO_4$, 0.1% BSA, and 0.1% glucose. Cells were rinsed twice with PS medium, prior to the LDL application. Cells were then incubated in PS medium containing 0.1 mg/mL DiI-LDL for 7 min at 37 °C, rinsed twice with PS medium, and incubated again for 1–3 h at 37 °C, 5% CO_2 in a cell incubator. Specific binding of LDL to LDL receptors was verified by observing the reduction in the fluorescence due to the DiI-LDL bound to cells upon incubation with a 10× molar excess of non-labeled LDL (Goldstein and Brown, 1976).

2.6. Treatment of cells with nocodazole, anti-motor antibodies, vanadate, and AMP-PNP

In order to depolymerize microtubules, cells were pretreated for 3 h in the presence of 10 μM nocodazole in PS medium before the addition of DiI-LDL. For antibody incorporation to cells, anti-dynein antibodies (clone 70.1) or anti-kinesin antibodies (clone SUK-4) were incorporated at 1:100 dilution for 15 min, from 45 min after the LDL pulse application, in the presence of 0.04% of saponin, with a modified lysis buffer consisted of 10 mM Na-HEPES (pH 7.0), 140 mM KCl, 1.8 mM $MgSO_4$, 2.4 mM NaH_2PO_4, 17.9 mM $NaHCO_3$, 2 mM EGTA, 5.6 mM glucose, and 1 mM ATP (Grundstrom et al., 1985; Ichikawa et al., 2000). Anti-dynein antibody (clone 70.1) used in the present study has previously been shown to inhibit cytoplasmic dynein in primary cultured astrocytes, resulting in endosome movement toward the cell periphery (Ichikawa et al., 2000). In melanophores, it has previously been reported that the application of either anti-dynein antibody (clone 70.1) or 50 μM of vanadate selectively inhibited retrograde motion, inducing melanosome dispersion by anterograde-directed kinesin bound to the same melanosomes (Nilsson and

Wallin, 1997). Anti-kinesin antibody SUK-4 has previously been reported to bind to kinesins, resulting in an acceleration of the centripetal motion of pigment granules in melanophores (Ingold et al., 1988; Rodionov et al., 1991). To inhibit dynein-like motor proteins, freshly prepared sodium orthovanadate (10, 30 or 50 μM) was added to cells at 45 min after the LDL pulse, in the presence of saponin in a modified lysis buffer. To inhibit kinesin-like motors, AMP-PNP (1 or 5 mM) was added to cells for 15 min, from 45 min after the LDL pulse, in the presence of saponin with a modified lysis buffer. After the incorporation of antibodies and inhibitors into cells, extracellular medium was replaced by PS medium. Saponin was used to render cell membranes permeable to the antibodies and inhibitors. All treatments of cells were performed at 37 °C.

2.7. Video-enhanced fluorescence microscopy

The intracellular endosome distribution was analyzed using a video-enhanced fluorescence microscope consisting of a Nikon inverted microscope (TMD-300, Japan) and an SIT camera (Hamamatsu Photonics C-1145, Japan). Glass-bottom dishes were mounted on the microscope, which was equipped with a constant-temperature chamber that maintained an air atmosphere at 37 °C. Data acquisition and image analysis were performed using an ARGUS-50 system (Hamamatsu Photonics). The video output was digitized and the images were stored in frame memory at a 512 × 483 pixel resolution. Excitation wavelengths of 450–490 and 510–560 nm were applied for Cy2 and DiI-LDL, respectively, and the resulting fluorescence was observed above 520 nm (Cy2), and above 590 nm (DiI). Wavelength selection was accomplished using filters, and either a DM510 dichroic mirror (Cy2), or a DM580 dichroic mirror (DiI). In the observation of microtubule distribution, deconvolution deblurring was performed with AutoDeblur software for the improvement of the image quality. The edge and nucleus of individual cells were revealed by phase-contrast observation.

2.8. Single endosome tracking analysis

The procedures necessary to track fluorescent particles through time-lapse imaging have been described elsewhere, in detail (Anderson et al., 1992). Each endosome containing DiI-LDL appeared as a spot covering a number of pixels, with diameter of 0.4–1.4 μm. Approximate endosome positions were estimated using a simple image analysis algorithm. Each endosome was subjected to a least-squares fit of the pixels in the endosome's immediate area with a two-dimensional Gaussian function, and the diameter of endosomes was then estimated from the measured width at 80% of maximal fluorescence intensity. Following this quantification procedure, the spots were linked through the time-lapse images, using a 'nearest spot with similar intensity' probability method. For the images obtained in this work, the observed particle densities were low, and distances between spots were typically larger than 1 μm. Although the algorithm must accept variations caused by photobleaching, endosomes demonstrated only small variations in fluorescence intensity from frame to frame. All generated tracks were operator-checked, and any track of doubtful validity was discarded from the subsequent analysis.

The directed motion of endosome i was represented in terms of a velocity vector, $\mathbf{V}_k{}^i$ (absolute velocity denoted by $V_k{}^i$), calculated at discrete-time intervals, $t(k) = k\delta t$, using the kth and $(k+1)$th images, where δt denotes the time interval between successive images. Formally,

$$\mathbf{V}_k^i = \frac{(\mathbf{r}_{k+1}^i - \mathbf{r}_k^i)}{\delta t} \quad (1)$$

$$V_k^i = \left|\mathbf{V}_k^i\right| \quad (2)$$

where $\mathbf{r}_k{}^i$ is the position vector of the ith endosome in the kth image. In the present tracking experiment, the choice of time interval ($\delta t = 1.2$ s) was restricted by the analog to digital data processing rate.

Individual endosome tracks were assigned as directed (including retrograde) motion along the microtubules (see Section 3). The minus end of each microtubule is anchored in the centrosome, near the nucleus, while the plus end is positioned near cell peripherals. Because microtubules have a curved, rather than linear overall structure, the orientation of a given microtubule is often not parallel to the vector from the respective cell peripheral to the nucleus. In order to quantitatively characterize the motion of endosome i towards the nucleus along its microtubule track, we calculated the centripetal velocity, $\mathrm{Vcp}_k{}^i$ by means of the inner product:

$$\mathrm{Vcp}_k^i = (\mathbf{V}_k^i, \mathbf{W}_i) \quad (3)$$

Here, $\mathbf{W}_i$ is a basis unit-vector from the initial position of the ith endosome to the center of cell nucleus. For determining the center of the nucleus, the edge of nucleus (revealed by phase-contrast imaging) was line-traced (resulting in the generation of a closed curve), and then the nucleic center was determined as the centroid of the closed curve.

When $\mathrm{Vcp}_k{}^i < 0$, the motion is peripherally directed one. In the present study, calculation of Vcp was performed for endosome tracks obtained by the 72 s observation from the indicated times.

2.9. Calculation of the degree of LDL-endosome concentration

The ratio of the total fluorescence intensity of the distinct, densely fluorescent regions about the centrosomes (their location was determined by staining with anti-tubulin antibodies) to the overall cellular fluorescence intensity was used to quantify the degree of concentration of DiI-LDL-containing endosomes in the vicinity of the nucleus.

2.10. Laser scanning confocal microscopy

A confocal microscope (Bio-Rad MRC-600UV, UK) equipped with an argon ion laser (Spectra-Physics Stabilite2016) was used to measure the three-dimensional distribution of LDL-containing endosomes in cells. This confocal microscope utilized the same Nikon inverted microscope as the video microscope. The fluorescence distribution of DiI-LDL was measured using an excitation wavelength of 514 nm, and observing the fluorescence above 550 nm. Wavelengths were selected using a 514DF10 excitation filter, a DR540LP dichroic reflector, and a 550LP emission filter.

2.11. Cytochemical staining and fluorescence imaging

Cell culture staining was performed at room temperature on glass-bottom dishes. After the fixation with 3% formalin for 30 min, cells were treated with an anti-microtubule antibody (10 μg/mL) in phosphate buffered saline (PBS, pH 7.4) for 90 min. Cells were then washed 10 times with PBS, and incubated with Cy2-conjugated goat anti-mouse antibody (0.10 mg/mL) for 30 min. Lysosomal staining was accomplished by adding acridine orange to cell cultures at a final concentration of 5 μg/mL. After 2 min, cells were rinsed twice with PS medium. Acridine orange fluorescence was observed using an excitation wavelength of 450–490 nm, and the fluorescence above 590 nm was monitored.

2.12. Western immunoblot

Cytoplasmic extracts were prepared by retaining the supernatant, following centrifugation (200,000 × g, 1 h, 4 °C) of homogenates from adrenocortical cells. The homogenization buffer was PBS (pH 7.4) with 0.05% Tween 20. The cytoplasmic extracts were treated with 6% SDS, and subjected to electrophoresis in 10% polyacrylamide gels. After transfer to polyvinylidene fluoride membranes (Immobilon-P; Millipore Co.), the blots were probed with the antibody against dynein (clone 70.1), or the antibody against kinesin (clone SUK-4), followed by incubation with biotinylated goat anti-mouse IgG. Finally, the membranes were incubated with streptavidin–horseradish peroxidase complex (Amersham). The protein bands were detected with ECL plus Western blotting detection reagents (Amersham).

2.13. Radioimmunoassay of steroidogenesis

Steroidogenic activities in adrenocortical cells were evaluated as PREG production measured with radioimmunoassay (RIA), which was performed as described elsewhere (Yamazaki et al., 1998). Adrenocortical cells cultured in a 24-well culture plate were incubated with a fresh medium containing PREG metabolism inhibitors, 2 μM trilostane and 20 μM SU-10603, in the presence/absence of 100 pM ACTH. After 2 h incubation of the cells under 5% CO_2 at 37 °C, accumulated PREG in the medium was extracted with hexane and measured by specific RIA.

2.14. Statistical analysis

Data are expressed as means ± SEM or means ± SD. Statistical significance was evaluated using two-tailed Student's t-test, with $P \leq 0.05$ as a criterion of significant difference.

3. Results

3.1. Centripetal movement and concentration of LDL-containing endosomes

The appearance of spherical endosomes, of diameter 0.4–1.4 μm, was observed at 20–30 min following the 7 min DiI-LDL pulse. In the following, the time of the completion of pulse labeling with DiI-LDL is designated as $t = 0$. At around $t = 30$–60 min after the LDL pulse addition, LDL-containing endosomes were distributed nearly uniformly over the entire cytoplasmic space (Fig. 1a and b). At $t = 30$ min, endosome diameter was distributed as follows: 0.4–0.6 μm (17.1%), 0.6–0.8 μm (41.6%), 0.8–1.0 μm (27.8%), and 1.0–1.4 μm (13.1%). Each endosome was observed to execute a saltatory motion, which consisted of forward and backward motions punctuated by immobile states, over the entire time

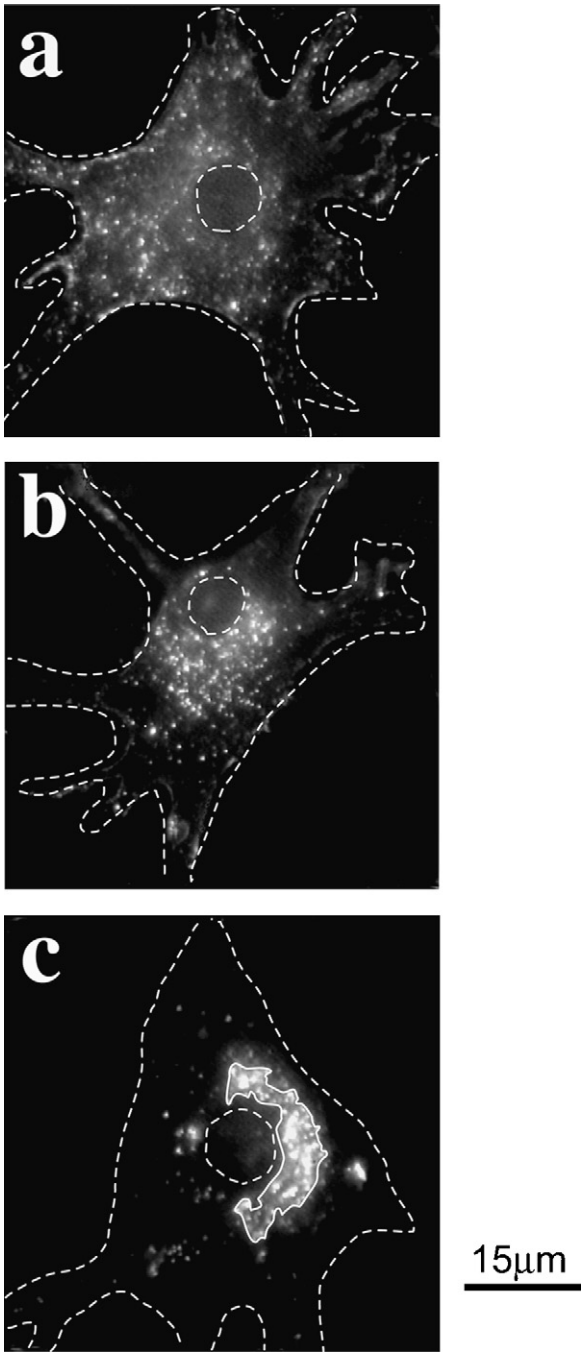

Fig. 1. Typical fluorescence images of the distribution of endosomes containing DiI-labeled LDL in adrenocortical cells. Cells were incubated for (a) 30 min, (b) 1 h and (c) 3 h at 37 °C after the pulse addition (7 min) of DiI-LDL, which was performed as described in Section 2. The endosomes appeared as fluorescent particles at $t = 30$ min (a). Diffused fluorescence observed in cytoplasmic space in (a) is probably derived from the optically undistinguishable very small vesicles containing DiI-LDL. At $t = 1$ h, the increase is observed in the number of the optically distinguishable endosomes, a large part of which are moving endosomal carrier vesicles (ECVs) (b). At $t = 3$ h, a large part of fluorescence are concentrated at perinuclear region, which are the result of the arrival of ECVs containing DiI-LDL to the late endosomes/lysosomes (c). The edges of the cell and nucleus are indicated by dotted lines in each image. In (c), the area enclosed by real line shows concentrated endosomes at the nuclear circumference. Scale bar = 15 μm.

range from $t = 30$ min to 3 h. The endosome population demonstrated a very slow, overall centripetal movement, resulting in the concentration of endosomes around the nuclear circumference, at $t = 3$ h (Fig. 1c). At $t = 1$ h, many endosomes were still moving in cytosolic region. To distinguish between early endosomes/ECVs and late endosomes/lysosomes, cells were doubly stained with DiI-LDL and acridine orange. The strong fluorescence of the endosome population at the nuclear circumference, due to acridine orange staining, indicates that most were late endosomes/lysosomes with an acidic pH of around 5. In contrast, moving endosomes still undergoing centripetal movement prior to reaching the perinuclear region, were not stained with acridine orange. No fusion of moving endosomes was observed.

3.2. Effect of the depolymerization of microtubules by nocodazole

To investigate the possibility of endosomal sliding on the microtubule networks, we examined the effect of a nocodazole-induced depolymerization of microtubules on endosome movement. After pre-incubating cells with 10 μM nocodazole for 3 h, DiI-LDL was added, and the endosome distribution was observed at $t = 3$ and 6 h. In nocodazole-treated cells, no significant concentration of endosomes around the circumference of nuclei was observed at either $t = 3$ or 6 h (Fig. 2a and b), although endosome formation was observed. No obvious difference on the endosome distribution was observed between $t = 3$ and 6 h. When nocodazole was removed by replacing the outer medium with the nocodazole-free PS medium, however, a significant concentration of endosomes around the nuclei was again observed, at 3 h after the nocodazole depletion (Fig. 2c). These results imply that endosomes undergo movement along microtubule networks. As shown in Fig. 3, the LDL-containing endosomes were placed on the microtubules.

The effect of actin filament disruption was also examined, in the presence of 100 nM cytochalasin D from $t = -15$ min, or from $t = 40$ min (after the formation of endosomes containing DiI-LDL). In pre-treated cells, the formation of endosomes was inhibited. When cytochalasin D was applied from $t = 40$ min, however, treated cells showed no difference from control cells, with respect to either endosome formation or their concentration around nuclei (data not shown). These results suggest that actin microfilaments are involved in endosome formation, but not in their subsequent movements about the cytosol.

3.3. Modulation of motor proteins with anti-motor protein antibodies and inhibitors

We investigated the contribution of both dynein-like and kinesin-like proteins to the motion of endosomes on microtubule networks. Inhibition of dynein-like motor proteins was accomplished by incubating cells with anti-dynein antibody (clone 70.1), as described in Section 2. This treatment prevented the concentration of endosomes around the nuclear circumference, resulting in the localization of endosomes around the cell periphery at $t = 3$ h (Fig. 4a). Western blotting of the cytoplasmic extracts of adrenocortical cells with anti-dynein antibody yielded a single band at approximately 70 kDa corresponding to a dynein intermediate chain, which might indicate the specificity of the anti-dynein antibody binding to dynein-like proteins. When the anti-dynein antibody was substituted to non-immunized serum (1:100), treated cells showed no apparent difference from control cells, with respect to either endosome formation or their concentration around nuclei (data not shown). The inhibition of dynein-like motor proteins was also accomplished using vanadate. In the presence of 10, 30 or 50 μM vanadate, we observed several peripheral concentrations of the LDL-containing endosomes at $t = 3$ h, with no significant concentration of endosomes around the circumference of nuclei (Fig. 4b). Under these conditions, no obvious change in the microtubule distribution was observed.

Inhibition of kinesin-like motor proteins was accomplished by incubating cells with anti-kinesin antibody (clone SUK-4). This treatment resulted in the concentration of endosomes around

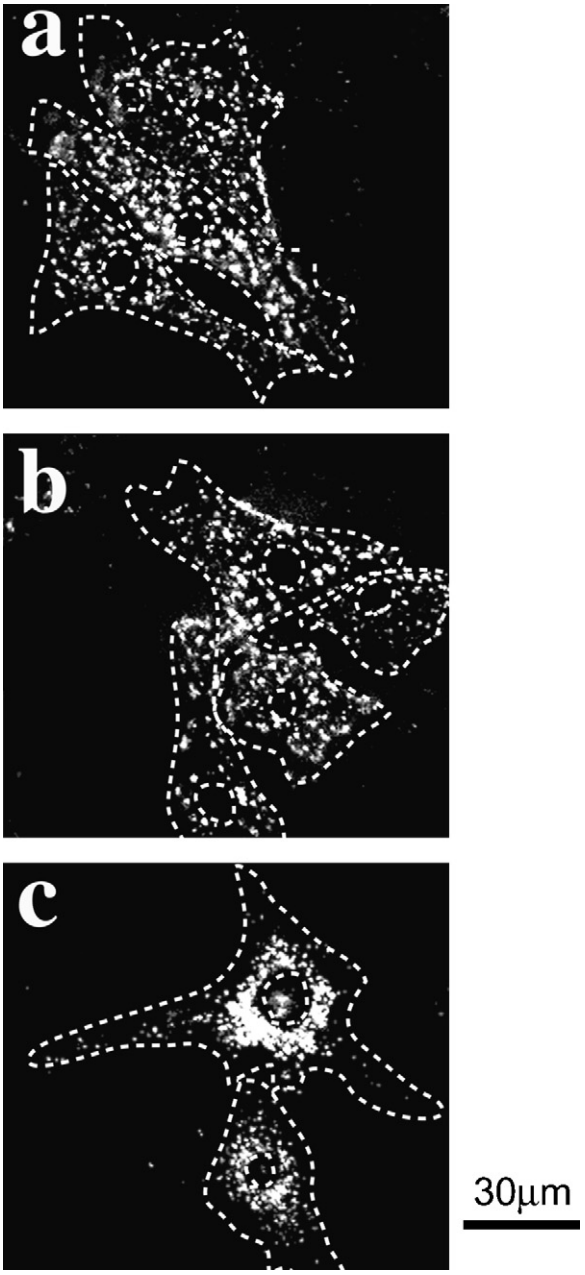

Fig. 2. Effect of the microtubule depolymerization by nocodazole on LDL-containing endosome distribution in adrenocortical cells. (a) Typical fluorescence image of nocodazole-treated cells at 3 h after the pulse application of DiI-LDL. Cells were pre-incubated with 10 μM nocodazole for 3 h, after which 7 min pulse application of DiI-LDL was performed as described in Section 2. Cells were then further incubated for 3 h in the presence of nocodazole. (b) Distribution of endosomes containing DiI-LDL after the additional 3 h incubation with 10 μM nocodazole. (c) Distribution of endosomes containing DiI-LDL after the additional 3 h incubation without nocodazole for once nocodazole-treated cells. Cells were washed with nocodazole-free PS medium and further incubated for 3 h in the absence of nocodazole. By the depletion of nocodazole, the re-polymerization of microtubules might occur, and the significant concentration of endosomes around the nuclei was observed again. The edges of the cell and nucleus are indicated by dotted lines in each image. Scale bar = 30 μm.

the circumference of nuclei at $t = 2$ h. The degree of endosomal perinuclear concentration induced by the application of anti-kinesin antibody at $t = 2$ h was similar to that observed in control cells at $t = 3$ h (Fig. 4d). The presence of kinesin-like proteins was demonstrated by Western blotting of the cytoplasmic extracts of adrenocortical cells, using anti-kinesin antibody, yielding a single band at approximately 130 kDa. The inhibition of kinesin-like

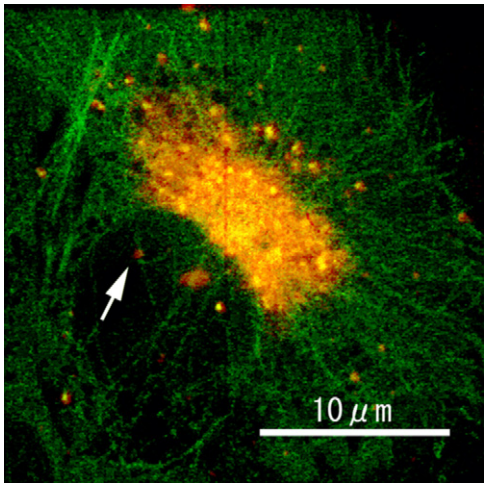

Fig. 3. Dual fluorescence labeling of LDL-containing endosomes (orange) and microtubules (green) in adrenocortical cells at 3 h after the application of DiI-LDL. Microtubules were immunostained with anti-alpha tubulin antibody and the Cy2-labeled secondary antibody as described in Section 2. Many endosomes are shown to be concentrated around the centrosome. The endosome indicated by an arrow is clearly placed on the microtubule. Scale bar = 10 μm. (For interpretation of the references to color in this figure legend, the reader is referred to the web version of the article.)

motors was also accomplished using AMP-PNP. In the presence of 1 mM AMP-PNP, endosomal movement in 30.5 ± 5.6% of the treated cells (mean ± SEM, $n = 6$, 26–31 cells were examined in each independent observation) was inhibited, resulting in a frozen, uniform distribution of endosomes in cytoplasmic space, with an endosome concentration around the nucleus of <20%. Application of 5 mM AMP-PNP resulted in the attainment of this frozen, uniform distribution by 93.8 ± 7.1% of the treated cells ($n = 6$, 29–36 cells were examined in each independent observation) (Fig. 4e).

That the 15 min saponin-treatment (used for the incorporation of antibodies and inhibitors) caused no disturbance to the endosome movement was verified by incubating cells, at $t = 45$ min, with a lysis buffer (containing 1 mM ATP) that mimics the cytosolic fluid (Fig. 4c and f). Essentially the same endosome concentration around the nuclei as previously observed was observed at $t = 3$ h.

3.4. Directed motion of individual endosomes with a period of retrograde motion along the microtubule networks

The details of individual endosome motion were investigated by single endosome tracking analysis. Fig. 5 shows typical trajectories of single endosomes in adrenocortical cells, over a time range of 72 s, starting at $t = 1$ h. Endosomes exhibited three different types of movement along the microtubules: forward motion, backward motion, and a temporarily immobile state.

The proportion of moving endosomes ($V_k{}^i \geq 0.065$ μm/s) to be 29.6 ± 4.9% and 75.2 ± 11.1%, at $t = 30$ min and 1 h, respectively (mean ± SD, $n = 18$ cells, 92–113 endosomes were analyzed in each cell). The remaining endosomes were either slowly moving or temporarily immobile (i.e. $V_k{}^i < 0.065$ μm/s) (see Fig. 6, closed bars). Most of the moving endosomes were transported bi-directionally (alternately forwards and backwards), with speeds of $V_k{}^i = 0.065$–0.260 μm/s (26.4 ± 4.8% at $t = 30$ min, 58.5 ± 10.5% at 1 h). Less than 3.3 ± 0.8% of the endosomes had a rate greater than $V_k{}^i = 0.26$ μm/s at $t = 30$ min. Many of the temporarily immobile endosomes also reverted to moving when we followed them over several additional tens of minutes, implying that they were not permanently immobile. Alternately, some moving endosomes became temporarily immobile, when tracked over a time range of several tens of minutes. The cutoff value of 0.065 μm was

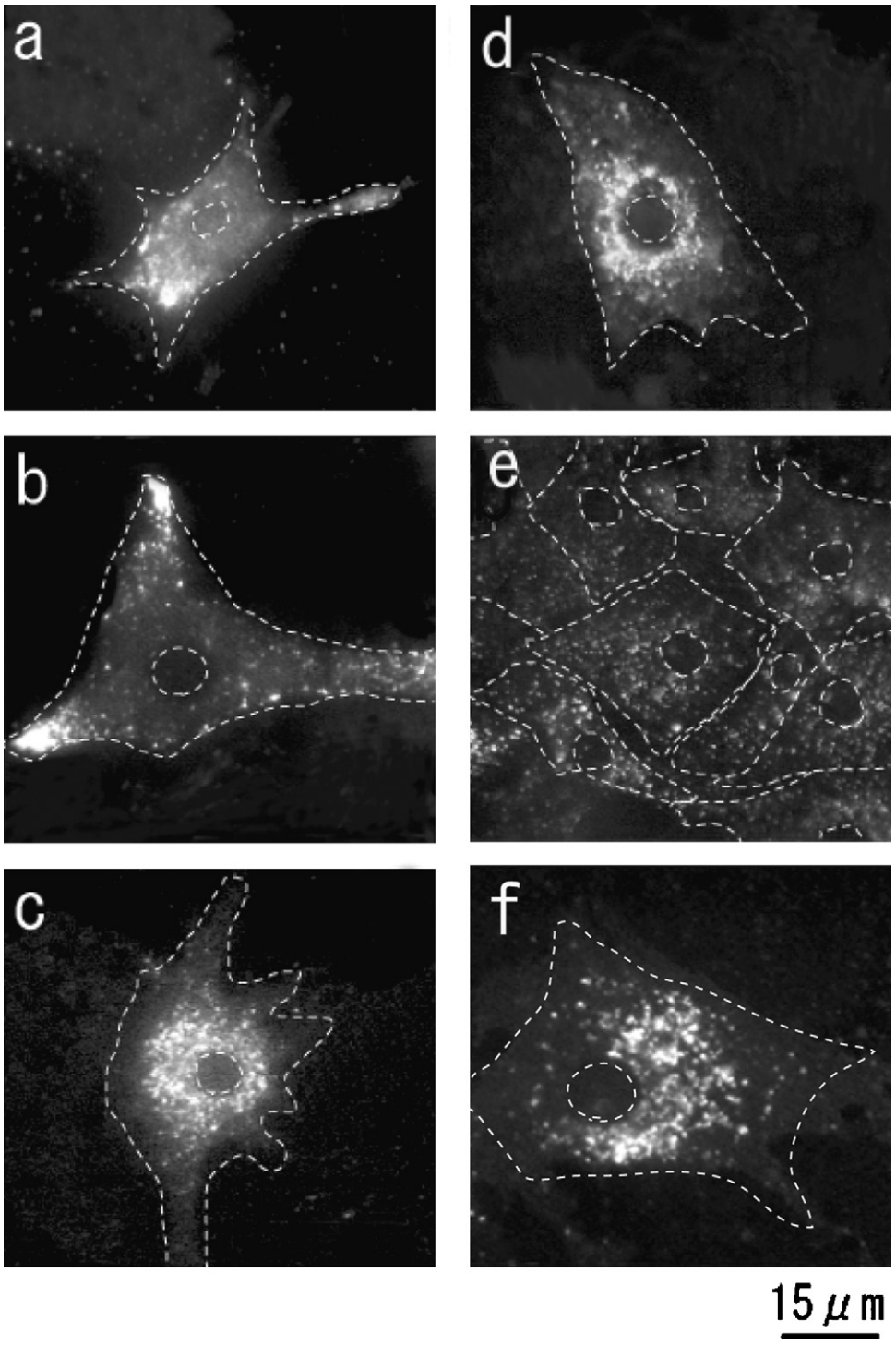

Fig. 4. Effects of antibodies and inhibitors of motor proteins on the distribution of endosomes. Incorporations of antibodies and inhibitors were carried out as described in Section 2. (a) In the presence of anti-dynein antibody at 3 h after the LDL addition. (b) In the presence of 50 μM vanadate at 3 h after the LDL addition. (c) In the absence of antibodies and inhibitors at 3 h after the LDL addition (control image to (a) and (b)). (d) In the presence of anti-kinesin antibody at 2 h after the LDL addition. (e) In the presence of 5 mM AMP-PNP at 2 h after the LDL addition. (f) In the absence of antibodies and inhibitors at 2 h after the LDL addition (control image to (d) and (e)). The edges of the cell and nucleus are indicated by dotted lines in each image. Scale bar = 15 μm. Note that the permeabilization by saponin was also performed in control cells ((c) and (f)).

essentially determined by the spacial resolution of our imaging system. Note that by employing the 2D-Gaussian fitting for endosomal positioning (see Section 2), we can detect the endosomal moving whose distance is below the 'optical resolution' comparable with a fluorescence wavelength. And note that the averaged velocity of endosome population over long time span could be much lower than 0.065 μm/s due to the bi-directional movements and the existence of the immobile population.

To quantitatively analyze the centripetal component of the motion of each endosome, calculation of the centripetal velocity, Vcp (see Eq. (3) in Section 2), was performed for endosome tracks obtained by the 72 s observation at $t = 30$ min and 1 h (Fig. 7, closed bars). Histograms of the endosome population vs. Vcp were

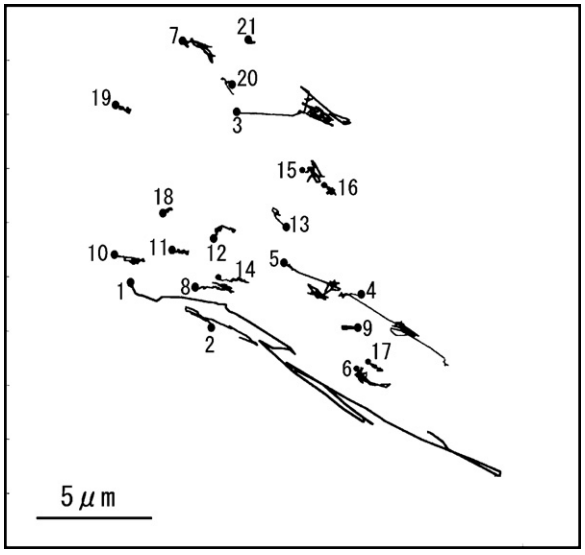

Fig. 5. Typical trajectories of single endosomes drawn by tracking endosomes for 61 successive images (72 s), with a time interval between images of 1.2 s. These images were taken from 1 h after the LDL addition in adrenocortical cells applied no inhibitors and drugs (the control condition). Endosomes exhibited three different types of movement along the microtubules: forward motion, backward motion, and a temporarily immobile state. Small filled circle represents the start point of each trace. The nucleus of the cell is placed in the lower right-hand corner.

well approximated by Gaussian distribution. Although the ratio of the endosomal population having positive Vcp to that having negative Vcp appeared to be nearly 1 in all analyzed cells, the averaged centripetal velocity of endosomes was greater than 0 (0.00305 ± 0.00008 μm/s at 30 min and 0.00198 ± 0.00007 μm/s at 1 h; mean ± SEM, $n = 18$ cells), indicating that centripetal velocity of the endosomal population was greater than the peripherally directed velocity.

3.5. Effect of ACTH on centripetal movement of endosomes

The application of 100 pM to 1 nM ACTH was observed to induce a significant increase in the rate of endosomal concentration around the circumference of cell nuclei. The time required for the concentration of endosomes around the nuclear circumference was shortened from 3 to 1 h by the application of 100 pM ACTH (compared with control unstimulated cells) (Fig. 8, Table 1). Using fluorescence double-staining (consisting of the immunostaining of both microtubules and DiI-LDL), we observed centrosomes located inside of these densely concentrated regions (Fig. 3). Following application of 100 pM and 1 nM ACTH, the fluorescent area concentrated around the centrosomes was 64.9 ± 4.5% (mean ± SEM, $n = 6$, 24–34 cells were examined in each independent observation) and 81.5 ± 5.6% ($n = 6$, each contained 27–36 cells), respectively, at $t = 1$ h. In control cells, the fraction of concentrated endosomes at $t = 1$ h was 26.1 ± 2.6% (c.f., 80.2 ± 5.9% at $t = 3$ h, $n = 6$, each contained 29–37 cells). Due to the high concentration of endosomes around nuclei in ACTH-stimulated cells, the surfaces of nuclei, observed using conventional fluorescence microscopy, often appeared to be covered by endosomes. Even in these cases, sliced images of varying vertical depth, obtained using confocal microscopy, indicated that the endosomes did not penetrate into the nuclei, but rather remained densely concentrated along the nuclear circumference. We also verified that no considerable change of cell shape had occurred.

Single endosome tracking analysis at $t = 30$ min and 1 h, indicated that ACTH increased the speed (absolute velocity) of endosomes by decreasing the population of immobile endosomes (see Fig. 6, open bars). At $t = 30$ min, the population of slowly moving or temporally immobile endosomes ($V_k{}^i < 0.065$ μm/s) was 70.4 ± 7.5% in control cells, but only 18.8 ± 5.3% in 100 pM ACTH-stimulated cells (mean ± SD, $n = 18$ cells, 83–109 endosomes were analyzed in each cell), demonstrating a significant decrease in the fraction of immobile endosomes. Analysis also indicated that ACTH-stimulation increased the velocity of moving endosomes. In ACTH-stimulated cells at $t = 30$ min, the population of endosomes having a velocity within 0.065–0.260 μm/s was 58.6 ± 7.1%, which was significantly greater than that in control cells (26.4 ± 4.8%). The population of rapidly moving endosomes ($V_k{}^i > 0.26$ μm/s) at $t = 30$ min was 22.6 ± 4.4% in ACTH-stimulated cells, which was also significantly greater than that (3.3 ± 0.8%) in unstimulated cells. At $t = 1$ h, the population of moving endosomes ($V_k{}^i \geq 0.065$ μm/s) became much smaller in ACTH-stimulated cells (15.4 ± 2.2%) than in control cells (75.2 ± 11.1%), because the majority of endosomes had already reached the perinuclear region, due to ACTH-stimulation.

To evaluate the centripetal component of the endosomal velocities, histograms of Vcp are shown in Fig. 7. In ACTH-stimulated cells, at $t = 30$ min, the fraction of endosomes with a net centripetal velocity (31.8 ± 4.2%) was significantly larger than that with a peripherally directed velocity (24.6 ± 3.9%). The rest was immobile. Upon ACTH-stimulation, the ratio of the number of centripetally moving endosomes to peripherally directed moving endosomes increased from 51.2:48.8 to 54.0:46.0, derived from the right-shift of the velocity distribution (Fig. 7). This indicates that ACTH selectively facilitated centripetal motion. The averaged centripetal velocity at $t = 30$ min in stimulated cells (Vcp = 0.00597 ± 0.00006 μm/s) was about 2-fold larger than that in control cells, which is consistent with imaging observations (Figs. 1 and 8). In stimulated cells, the averaged centripetal velocity at $t = 1$ h was nearly 0 (−0.00001 ± 0.00002 μm/s), due to the high concentration of endosomes in perinuclear regions.

Table 1
Degree of endosomal concentration (%) around centrosomes at 1 or 3 h after the LDL addition in the presence of stimuli and/or Ca^{2+} chelators.

	1 h	3 h
Control	26.1 (2.6)[a]	80.2 (5.9)
ACTH	64.9 (4.5)*	79.6 (3.7)
ACTH + EGTA	28.0 (3.6)	72.7 (1.7)
ACTH + BAPTA	39.1 (6.2)**	49.4 (7.2)*
ACTH + EGTA + BAPTA	24.4 (4.3)	33.7 (2.4)**
Forskolin	29.6 (2.3)	68.3 (2.1)

Concentrations of chemicals were 100 pM ACTH, 2 mM EGTA, 5 μM BAPTA/AM and 1 μM forskolin. Quantification of endosomal concentration was performed as described in Section 2. The application of stimuli and/or Ca^{2+} chelators was performed just after the completion of DiI-LDL labeling ($t = 0$).

[a] SEM.

* $P < 0.05$, ** $P < 0.01$ vs control, evaluated from six independent experiments.

3.6. Involvement of Ca^{2+} in ACTH-induced endosome concentration

The ACTH-induced acceleration of endosome concentration around the nuclear circumference was inhibited by the chelation of extracellular and intracellular Ca^{2+} (Table 1). This chelation was accomplished by adding 2 mM EGTA and/or 5 μM BAPTA/AM to the external cell medium. The depletion of extracellular Ca^{2+} by EGTA reduced the observed endosomal concentration around nuclear circumference, at $t = 1$ h from 64.9% to 28.0%. Similarly, intracellular Ca^{2+} chelation using BAPTA reduced the concentration to 39.1%. When both extracellular and intracellular Ca^{2+} were chelated, only 24.4% of the endosomes were concentrated around the nuclei at $t = 1$ h. Note that this inhibition of the ACTH effect by Ca^{2+} chelation was also observed at $t = 3$ h.

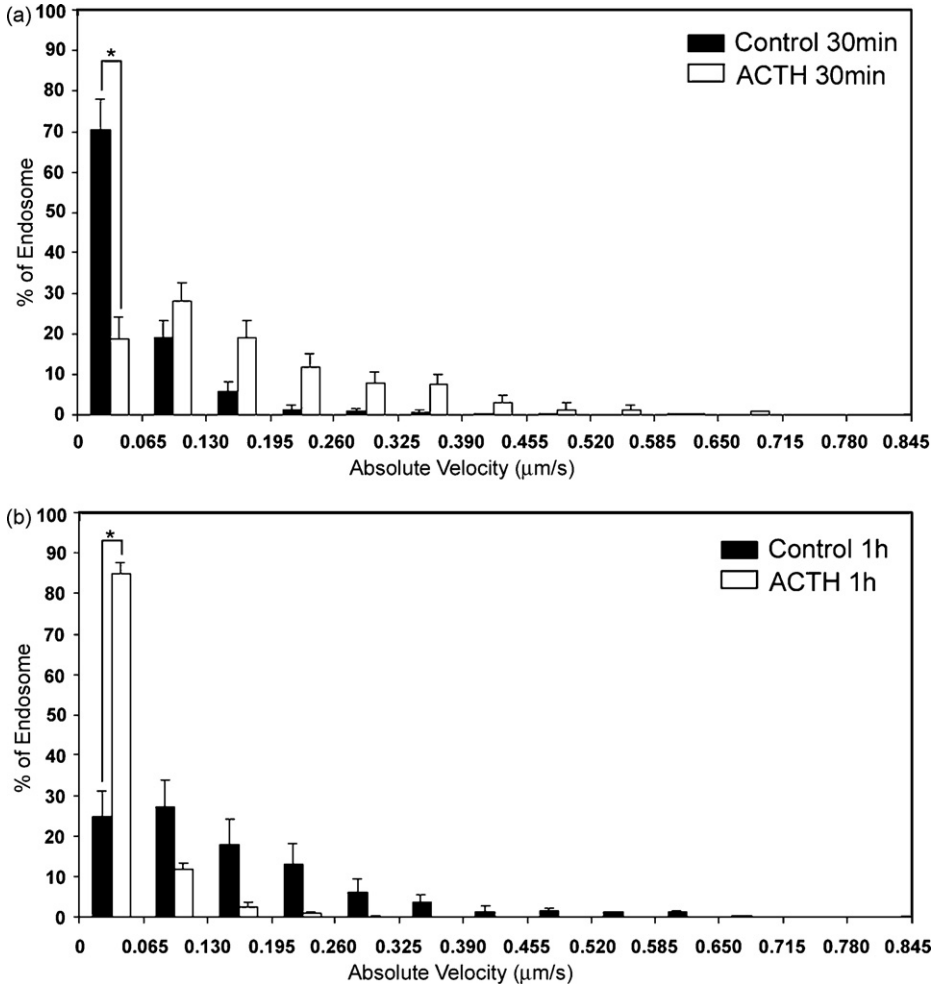

Fig. 6. The absolute velocity distribution (V_k^i) of single endosomes at 30 min (panel a) and 1 h (panel b) after the pulsed LDL addition in control (unstimulated) cells (closed bar, $n = 18$ cells from several independent experiments) and in 100 pM ACTH-stimulated cells (open bar, $n = 18$ cells). ACTH application started just after the completion of DiI-LDL labeling ($t = 0$). Absolute velocity was calculated using Eqs. (1) and (2) in Section 2. 92–113 and 83–109 endosomes were analyzed in each cell under the control condition and the ACTH-treated condition, respectively. At $t = 30$ min, the population of slowly moving or temporally immobile endosomes (0.000–0.065 μm/s) in ACTH-treated cells was significantly decreased than that in control cells. On the other hand, the population of slowly moving or temporally immobile endosomes in ACTH-treated cells was significantly increased than that in control cells at $t = 1$ h, because the majority of the endosomes had already reached the nuclei in ACTH-stimulated cells. Error bars are SD. $^*P \leq 0.05$ vs. control.

To investigate the possible involvement of cAMP in ACTH effect, we applied forskolin, an adenyl cyclase activator, to adrenocortical cells. The addition of 1 μM forskolin resulted in a perinuclear endosome concentration of 29.6%, at $t = 1$ h, a result similar to that observed in control cells. In addition, the direct incorporation of 1 μM cAMP to cells permeabilized with saponin resulted in almost no facilitation of perinuclear endosome concentration.

3.7. Steroidogenic activity of adrenocortical cells

PREG production was measured in order to monitor the activity of adrenocortical cells used for imaging investigations. In control adrenocortical cells, basal PREG production was determined to be 0.52 ± 0.01 nmol/mg protein/2 h by means of RIA ($n = 3$, each performed in triplicate). Upon stimulation with 100 pM ACTH, PREG production was increased to 4.46 ± 0.18 nmol/mg protein/2 h ($n = 3$). LDL application did not significantly change the PREG production within 5% for 2 h.

4. Discussion

The current investigation focuses on the analysis of the intracellular transport of LDL by endosomes. LDL-containing endosomes accomplish the long-distance transport of cholesteryl esters across the cytoplasmic space, while the movements of the early and the late endosomes/lysosomes are relatively small, in comparison. The spherical shape and the diameter of moving endosomes (0.4–1.4 μm in most endosomes) were essentially in accordance with the properties of ECVs previously reported in other kind of cells (Griffiths, 1996). No fusion of moving endosomes was observed, which is again in accordance with the ECVs' character. However, almost all moving endosomes containing fluorescent LDL were not stained with acridine orange, suggesting that in LDL-containing endosomes the significant pH reduction might not occur. It is different from the case of transferrin-transporting ECVs in chicken erythroblast cells, in which a marked decrease in pH (to 5–5.5) was observed (Killisch et al., 1992). The regulation of pH in endosomes might be dependent on cell species and/or transporting materials.

Application of ACTH was shown to shorten the time required for LDL-containing endosomes to travel from the cytoplasm to the circumference of the nuclei from 3 h (in control cells) to 1 h (ACTH-stimulated cells). Single endosome tracking analysis indicates that this effect was due to increases in the centripetal velocity, and in the fraction of mobile endosomes (see Fig. 6). This is the first demonstration of the hormonal regulation for

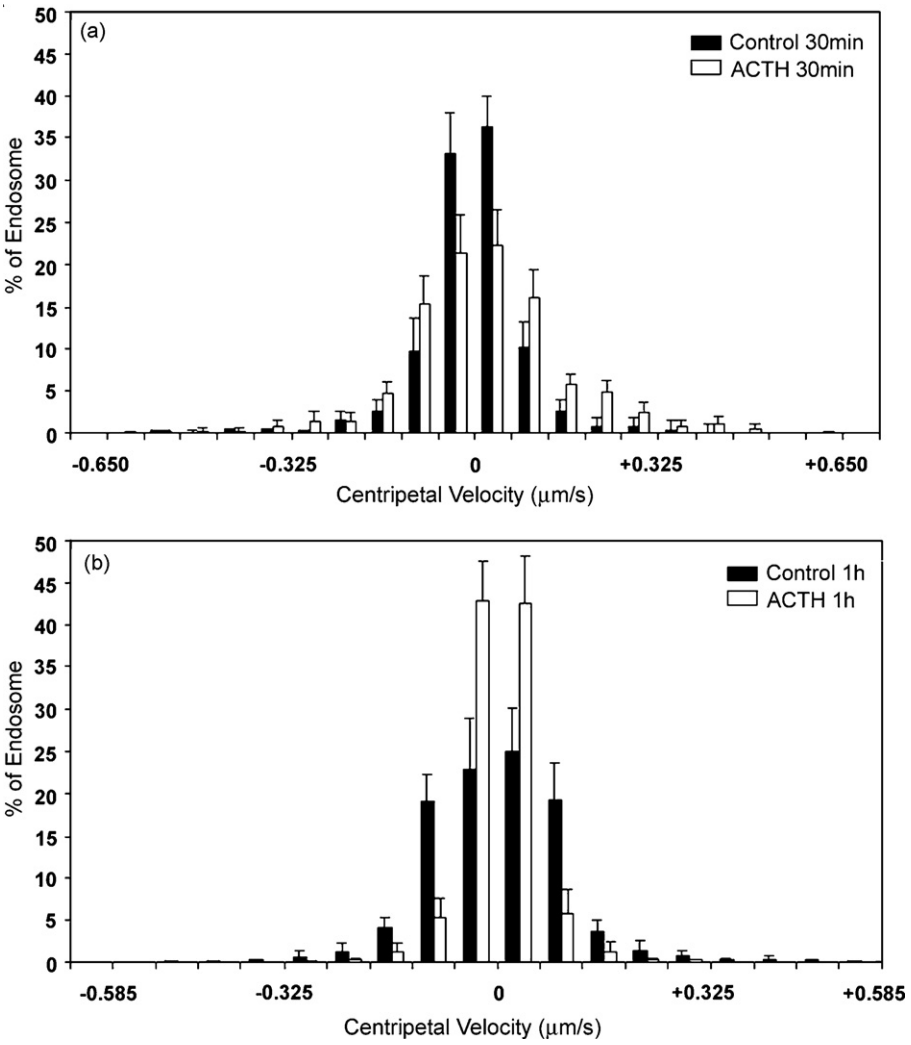

Fig. 7. The centripetal velocity (Vcp) distribution of single endosomes at 30 min (panel a) and 1 h (panel b) after the pulsed LDL addition in control (unstimulated) cells (closed bar, $n = 18$ cells from several independent experiments) and in 100 pM ACTH-stimulated cells (open bar, $n = 18$ cells). ACTH application started just after the completion of DiI-LDL labeling ($t = 0$). Vcp was calculated using Eq. (3) in Section 2. 92–113 and 83–109 endosomes were analyzed in each cell under the control condition and the ACTH-treated condition, respectively. Plus and minus values correspond to the velocity of centripetal motion and peripherally directed motion, respectively. Error bars are SD.

the intracellular LDL-cholesteryl ester traffic in adrenocortical cells.

In the present study, we demonstrate that although many individual endosomes undergo rapid movement (typically 0.065–0.260 μm/s), the establishment of a high concentration of endosomes about the nuclear circumference requires almost 3 h, following pulsed LDL addition. This paradoxical phenomenon is the result of the saltatory nature (i.e. forward and backward) of endosomal motions.

4.1. Endosome movement is driven by both dynein and kinesin-like motors along microtubule networks

We examined the involvement of microtubule-based motor proteins in driving endosome movements. The inhibition of dynein-like motor proteins by the application of dynein antibodies or vanadate prevented the centripetal endosomal motion and facilitated anti-centripetal (peripherally directed) motion driven by kinesin-like motor proteins. On the other hand, the inhibition of kinesin-like motors by the application of anti-kinesin antibody prevented the peripherally directed motion and caused facilitated centripetal motion by dynein-like motor proteins. These results are consistent only if both dynein-like and kinesin-like proteins are bound to the same endosome, as previously shown for endosomes in astrocytes (Ichikawa et al., 2000) and pigment granules in melanophores (Ingold et al., 1988; Rodionov et al., 1991). The view that endosomes contain both dynein and kinesin motors is also consistent with our observation that moving endosomes frequently altered their direction in the motion. Endosomes that remain immobile over a short time span of several minutes are probably detached from the microtubules. Saltatory motion of the single endosome might occur in the following mechanisms: In the course of sliding on microtubule rails, an endosome may dissociate from those in some probabilities by heat-dynamic fluctuation. If kinesin-like motor protein, instead of dynein, is employed in endosomal re-association to microtubules, the endosome might be transported toward peripheral direction. If dynein is responsible for the re-association, the movement in the opposite direction may occur. The recruitment of both motors might occur in the stochastic manner, resulting in the random walk-like motions of the endosome. The net centripetal motion of endosomal population might reflect the greater number of dynein-like proteins bound to the single endosome than that of kinesin-like proteins. Because AMP-PNP, a non-hydrolysable ATP analogue, caused a tight attachment

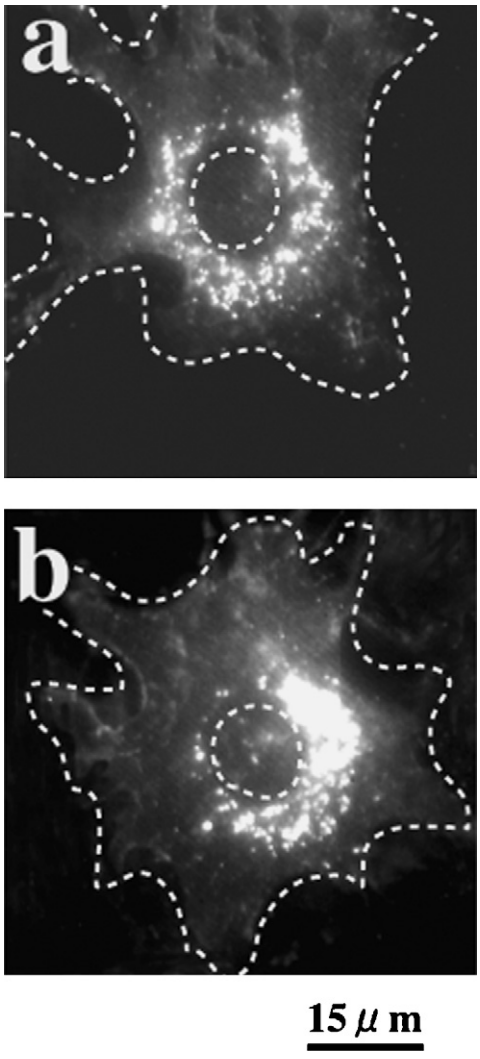

Fig. 8. ACTH-induced facilitation of the concentration of endosomes around nuclei. Typical fluorescence images of LDL-containing endosome distribution at 30 min (panel a) and 1 h (panel b) after the pulse DiI-LDL addition in the presence of 100 pM ACTH. ACTH application started just after the completion of DiI-LDL labeling ($t = 0$). The edges of the cell and nucleus are indicated by dotted lines in each image. Scale bar = 15 μm.

between kinesin-like proteins and the microtubules (Block et al., 1990), the application of AMP-PNP prevented both the centripetal and peripherally directed motions of LDL-containing endosomes, resulting in the frozen uniform distribution. Although the biological meaning of bi-directional saltatory motion is still unclear, the bi-directional transport of organelles is not a special case for LDL-containing endosomes in adrenocortical cells. For example, Rogers et al. (1997) demonstrated the bi-directional motility of melanophore along microtubules driven by the plus end-directed motor, kinesin-2 and the minus end-directed motor, cytoplasmic dynein.

The slow net velocities of endosome population (0.00305 μm/s at $t = 30$ min and 0.00198 μm/s at $t = 1$ h, over a long time scale) explain why endosomes require nearly 3 h to reach the nuclear circumference, a journey which involves the movement of approximately 20 μm from the cell periphery, in a sum of forward, backward and immobile movements. Such a very slow average movement results in a slightly greater probability of centripetal, rather than peripherally directed movement. The ratio of the number of centripetal moving endosomes to peripherally directed moving endosomes was 51.2:48.8 in the absence of ACTH. This small difference between centripetal and peripherally directed movements has a physiological relevance. When we assume that the relative ratio of the population of endosomes with a centripetal motion to peripherally directed motion is, for example, 51:49, 52:48 or 53:47, in addition we also assume that endosomes have the same rate of 0.1 μm/s with changing directions frequently, then, time required for the perinuclear accumulation of endosomes are approximately 2.9, 1.4 and 0.9 h, respectively (e.g. when the ratio is 51:49, the average centripetal velocity over a distance of 20 μm is $0.51 \times 0.1 - 0.49 \times 0.1 = 0.002$ μm/s = 7 μm/h, reaching the goal after approximately 2.9 h). This discussion explains that such a small difference of 51:49 could results in a 3 h journey for endosomes to reach nuclei. ACTH-stimulation was observed to increase the ratio to be 54.0:46.0, which seemed to be also approximately consistent with the result that ACTH caused the shortening of the time required for the endosomal accumulation from 3 to 1 h.

LDL-containing endosomes were observed to fuse finally to the late endosomes/lysosomes locating at the perinuclear region, in which the degradation of endosomes and the liberation of DiI-LDL might occur, which was judged from the diffused fluorescence distribution at the region. Although the direct contact of LDL-containing endosomes to steroidogenic mitochondria cannot be completely excluded, it seems not to be plausible in the perinuclear region, since P450scc-containing mitochondria are sparse in the region of bovine adrenal fasciculata cells (Kimoto et al., 1997).

4.2. ACTH-stimulative effects may require the intracellular and extracellular Ca^{2+}

When extracellular Ca^{2+} was depleted, ACTH induced almost no facilitation of perinuclear endosome concentration, probably due to the suppression of ACTH-induced Ca^{2+} signals. Physiological concentrations of ACTH (1–10 pM) have been demonstrated to evoke Ca^{2+} signals in adrenal fasciculata cells (Kimoto et al., 1996, 1997; Yamazaki et al., 1998, 2006). The depletion of the extracellular Ca^{2+}, by which the ACTH-induced facilitation in endosomal perinuclear accumulation was suppressed, was also shown to attenuate ACTH-induced Ca^{2+} signaling in adrenal fasciculata cells. Although the binding affinity of ACTH to its receptors was reported to be Ca^{2+}-dependent in old study (Cheitlin et al., 1985), the conflict data was offered in recent study (Gallo-Payet et al., 1996) showing that Ca^{2+} was not required for ACTH binding. Furthermore, the depletion of the extracellular Ca^{2+} inhibited the facilitation of endosomal perinuclear concentrations evoked by ACTH in 1 nM which was 1000-fold higher concentration required for the induction of Ca^{2+} signaling. Therefore, it was not plausible that the Ca^{2+} depletion-induced suppression of the ACTH effect was due to the prevention of the ACTH binding to its receptors. The inhibitory effect of BAPTA chelating intracellular Ca^{2+} and suppressing the ACTH-induced Ca^{2+} signaling was also supportive to our conclusion. Taken together, these results indicate that Ca^{2+} signals are required for the ACTH-induced facilitation of endosomal perinuclear concentration.

The potential contribution of cAMP pathway to ACTH-induced effects is still unclear. Since we observed no facilitation in the perinuclear endosome concentration, either by the application of 1 μM forskolin or by the direct incorporation of 1 μM cAMP into the cell cytoplasm, at least this level of the cytosolic cAMP appeared to have little effect in the facilitation of endosomal accumulation. However, since the higher concentration of ACTH than 100 pM could elicit the higher cytosolic cAMP than 1 μM, the possibility cannot be completely excluded that the higher concentration of cAMP which might be induced by the extremely high concentration of ACTH may be effective, as shown in the case for melanosome dispersion that was facilitated by exogenous cAMP addition with saponin-treatment (Grundstrom et al., 1985).

Although further studies will be needed for the elucidation of precise molecular mechanisms by which ACTH and Ca^{2+} govern the traffic of LDL-containing endosomes in adrenocortical cells, protein kinase C or Ca^{2+}/calmodulin kinase pathways, which have been shown to be activated by ACTH (Nishikawa et al., 1996; Yamazaki et al., 2006), might be possible candidates for regulative factors, as suggested in the regulation of dynein-dependent vesicle transport in fibroblast (Hayden, 1988).

In conclusion, in the present study, the novel regulation by ACTH for the intracellular cholesterol transport via LDL was demonstrated in adrenocortical cells. ACTH-induced acceleration of LDL transport was accomplished predominantly by increasing the rate of individual endosomal moving and the increase of the moving population of LDL-containing endosomes. The moving endosomes contained both dynein-like and kinesin-like motor proteins, by which bidirectional and salutatory motion was achieved.

Acknowledgments

We thank Prof. T. Yamazaki at Hiroshima University for his kind donation of anti-PREG antibodies. We also thank to Mochida Pharmaceutical Corp. and Novartis for their donations of trilostane and SU-10603, respectively. This work was supported by grants from the Ministry of Education, Science and Culture in Japan and by BBSRC in the UK. This work was also supported by grants from CREST Project of JPST for "Endocrine Disruption on Action of Brain Neurosteroids". We thank Prof. John Rose (Ritsumeikan University) for reading of the manuscript.

References

Anderson, C.M., Georgiou, G.N., Morrison, I.E., Stevenson, G.V., Cherry, R.J., 1992. Tracking of cell surface receptors by fluorescence digital imaging microscopy using a charge-coupled device camera. Low-density lipoprotein and influenza virus receptor mobility at 4 degrees C. J. Cell. Sci. 101 (Pt 2), 415–425.

Block, S.M., Goldstein, L.S., Schnapp, B.J., 1990. Bead movement by single kinesin molecules studied with optical tweezers. Nature 348, 348–352.

Cavallaro, S., Pani, L., Guidotti, A., Costa, E., 1993. ACTH-induced mitochondrial DBI receptor (MDR) and diazepam binding inhibitor (DBI) expression in adrenals of hypophysectomized rats is not cause-effect related to its immediate steroidogenic action. Life Sci. 53, 1137–1147.

Cheitlin, R., Buckley, D.I., Ramachandran, J., 1985. The role of extracellular calcium in corticotropin-stimulated steroidogenesis. J. Biol. Chem. 260, 5323–5327.

Connelly, M.A., Williams, D.L., 2003. SR- BI and cholesterol uptake into steroidogenic cells. Trends Endocrinol. Metab. 14, 467–472.

Dietschy, J.M., Kita, T., Suckling, K.E., Goldstein, J.L., Brown, M.S., 1983. Cholesterol synthesis in vivo and in vitro in the WHHL rabbit, an animal with defective low density lipoprotein receptors. J. Lipid Res. 24, 469–480.

Gallo-Payet, N., Grazzini, E., Cote, M., Chouinard, L., Chorvatova, A., Bilodeau, L., Payet, M.D., Guillon, G., 1996. Role of Ca^{2+} in the action of adrenocorticotropin in cultured human adrenal glomerulosa cells. J. Clin. Invest. 98, 460–466.

Ghosh, R.N., Maxfield, F.R., 1995. Evidence for nonvectorial, retrograde transferrin trafficking in the early endosomes of HEp2 cells. J. Cell Biol. 128, 549–561.

Glass, C., Pittman, R.C., Weinstein, D.B., Steinberg, D., 1983. Dissociation of tissue uptake of cholesterol ester from that of apoprotein A-I of rat plasma high density lipoprotein: selective delivery of cholesterol ester to liver, adrenal, and gonad. Proc. Natl. Acad. Sci. U.S.A. 80, 5435–5439.

Glick, D., Ochs, M.J., 1955. Studies in histochemistry: quantitative histological distribution of cholesterol in adrenal glands of the cow, rat and monkey, and effects of stress conditions, ACTH, cortisone and deoxycorticosterone. Endocrinology 56, 285–298.

Goldstein, J.L., Brown, M.S., 1976. The LDL pathway in human fibroblasts: a receptor-mediated mechanism for the regulation of cholesterol metabolism. Curr. Top. Cell Regul. 11, 147–181.

Grahame-Smith, D.G., Butcher, R.W., Ney, R.L., Sutherland, E.W., 1967. Adenosine 3' 5'-monophosphate as the intracellular mediator of the action of adrenocorticotropic hormone on the adrenal cortex. J. Biol. Chem. 242, 5535–5541.

Griffiths, G., 1996. On vesicles and membrane compartments. Protoplasma 195, 37–58.

Grundstrom, N., Karlsson, J.O., Andersson, R.G., 1985. The control of granule movement in fish melanophores. Acta Physiol. Scand. 125, 415–421.

Havel, R.J., Eder, H.A., Bragdon, J.H., 1955. The distribution and chemical composition of ultracentrifugally separated lipoproteins in human serum. J. Clin. Invest. 34, 1345–1353.

Hayden, J.H., 1988. Microtubule-associated organelle and vesicle transport in fibroblasts. Cell Motil. Cytoskeleton. 10, 255–262.

Heikkila, P., Kahri, A.I., Ehnholm, C., Kovanen, P.T., 1989. The effect of low- and high-density lipoprotein cholesterol on steroid hormone production and ACTH-induced differentiation of rat adrenocortical cells in primary culture. Cell Tissue Res. 256, 487–494.

Herman, B., Albertini, D.F., 1984. A time-lapse video image intensification analysis of cytoplasmic organelle movements during endosome translocation. J. Cell Biol. 98, 565–576.

Ichikawa, T., Yamada, M., Homma, D., Cherry, R.J., Morrison, I.E., Kawato, S., 2000. Digital fluorescence imaging of trafficking of endosomes containing low-density lipoprotein in brain astroglial cells. Biochem. Biophys. Res. Commun. 269, 25–30.

Ingold, A.L., Cohn, S.A., Scholey, J.M., 1988. Inhibition of kinesin-driven microtubule motility by monoclonal antibodies to kinesin heavy chains. J. Cell Biol. 107, 2657–2667.

Iwaki, T., Noguchi, A., Sekimoto, T., 1985. Sources of extramitochondrial corticoidogenic cholesterol in the adrenal cortex. Jpn. J. Pharmacol. 38, 207–214.

Jacobson, L., 2005. Hypothalamic–pituitary–adrenocortical axis regulation. Endocrinol. Metab. Clin. North Am. 34, 271–292, vii.

Killisch, I., Steinlein, P., Romisch, K., Hollinshead, R., Beug, H., Griffiths, G., 1992. Characterization of early and late endocytic compartments of the transferrin cycle Transferrin receptor antibody blocks erythroid differentiation by trapping the receptor in the early endosome. J. Cell Sci. 103 (Pt 1), 211–232.

Kimoto, T., Ohta, Y., Kawato, S., 1996. Adrenocorticotropin induces calcium oscillations in adrenal fasciculata cells: single cell imaging. Biochem. Biophys. Res. Commun. 221, 25–30.

Kimoto, T., Ohta, Y., Kawato, S., 1997. Heterogeneous populations of adrenal fasciculata cells examined with Ca^{2+} signaling and immunostaining: single cell imaging. Bioimages 5, 133–142.

Kimura, T., 1981. ACTH stimulation on cholesterol side chain cleavage activity of adrenocortical mitochondria. Transfer of the stimulus from plasma membrane to mitochondria. Mol. Cell. Biochem. 36, 105–122.

King, S.R., Ronen-Fuhrmann, T., Timberg, R., Clark, B.J., Orly, J., Stocco, D.M., 1995. Steroid production after in vitro transcription, translation, and mitochondrial processing of protein products of complementary deoxyribonucleic acid for steroidogenic acute regulatory protein. Endocrinology 136, 5165–5176.

Kovanen, P.T., Faust, J.R., Brown, M.S., Goldstein, J.L., 1979. Low density lipoprotein receptors in bovine adrenal cortex. I. Receptor-mediated uptake of low density lipoprotein and utilization of its cholesterol for steroid synthesis in cultured adrenocortical cells. Endocrinology 104, 599–609.

Kraemer, F.B., Shen, W.J., Patel, S., Osuga, J., Ishibashi, S., Azhar, S., 2007. The LDL receptor is not necessary for acute adrenal steroidogenesis in mouse adrenocortical cells. Am. J. Physiol. Endocrinol. Metab. 292, E408–412.

Kroon, P.A., Thompson, G.M., Chao, Y.S., 1984. A comparison of the low-density-lipoprotein receptor from bovine adrenal cortex, rabbit and rat liver and adrenal glands by lipoprotein blotting. Biochem. J. 223, 329–335.

Li, H., Brochu, M., Wang, S.P., Rochdi, L., Cote, M., Mitchell, G., Gallo-Payet, N., 2002. Hormone-sensitive lipase deficiency in mice causes lipid storage in the adrenal cortex and impaired corticosterone response to corticotropin stimulation. Endocrinology 143, 3333–3340.

Massotti, M., Slobodyansky, E., Konkel, D., Costa, E., Guidotti, A., 1991. Regulation of diazepam binding inhibitor in rat adrenal gland by adrenocorticotropin. Endocrinology 129, 591–596.

Nilsson, H., Wallin, M., 1997. Evidence for several roles of dynein in pigment transport in melanophores. Cell Motil. Cytoskeleton 38, 397–409.

Nishikawa, T., Sasano, H., Omura, M., Suematsu, S., 1996. Regulation of expression of the steroidogenic acute regulatory (StAR) protein by ACTH in bovine adrenal fasciculata cells. Biochem. Biophys. Res. Commun. 223, 12–18.

Paavola, L.G., Strauss, J.F.3rd, Boyd, C.O., Nestler, J.E., 1985. Uptake of gold- and [3H]cholesteryl linoleate-labeled human low density lipoprotein by cultured rat granulosa cells: cellular mechanisms involved in lipoprotein metabolism and their importance to steroidogenesis. J. Cell Biol. 100, 1235–1247.

Rainey, W.E., Rodgers, R.J., Mason, J.I., 1992. The role of bovine lipoproteins in the regulation of steroidogenesis and HMG-CoA reductase in bovine adrenocortical cells. Steroids 57, 167–173.

Rodionov, V.I., Gyoeva, F.K., Gelfand, V.I., 1991. Kinesin is responsible for centrifugal movement of pigment granules in melanophores. Proc. Natl. Acad. Sci. U.S.A. 88, 4956–4960.

Rogers, S.L., Tint, I.S., Fanapour, P.C., Gelfand, V.I., 1997. Regulated bidirectional motility of melanophore pigment granules along microtubules in vitro. Proc. Natl. Acad. Sci. U.S.A. 94, 3720–3725.

Simpson, E.R., Waterman, M.R., 1983. Regulation by ACTH of steroid hormone biosynthesis in the adrenal cortex. Can. J. Biochem. Cell Biol. 61, 692–707.

Stocco, D.M., Clark, B.J., 1996. Regulation of the acute production of steroids in steroidogenic cells. Endocr. Rev. 17, 221–244.

Yaguchi, H., Tsutsumi, K., Shimono, K., Omura, M., Sasano, H., Nishikawa, T., 1998. Involvement of high density lipoprotein as substrate cholesterol for steroidogenesis by bovine adrenal fasciculo-reticularis cells. Life Sci. 62, 1387–1395.

Yamazaki, T., Kimoto, T., Higuchi, K., Ohta, Y., Kawato, S., Kominami, S., 1998. Calcium ion as a second messenger for o-nitrophenylsulfenyl-adrenocorticotropin (NPS-ACTH) and ACTH in bovine adrenal steroidogenesis. Endocrinology 139, 4765–4771.

Yamazaki, T., Kawasaki, H., Takamasa, A., Yoshitomi, T., Kominami, S., 2006. Ca^{2+} signal stimulates the expression of steroidogenic acute regulatory protein and steroidogenesis in bovine adrenal fasciculata-reticularis cells. Life Sci. 78, 2923–2930.